Asymptotically exact formulas for the stripe domains period in ultrathin ferromagnetic films with out-of-plane anisotropy

Anne Bernand-Mantel, Valeriy V. Slastikov, Cyrill B. Muratov

Asymptotically exact formulas for the stripe domains period in ultrathin ferromagnetic films with out-of-plane anisotropy

Anne Bernand-Mantel,[1,*] Valeriy V. Slastikov,[2] and Cyrill B. Muratov[3]

[1] *Centre d'Elaboration de Matériaux et d'Etudes Structurales, CEMES-CNRS, 29 rue Jeanne Marvig, 31055 Toulouse, France*
[2] *School of Mathematics, University of Bristol, Bristol BS8 1UG, United Kingdom*
[3] *Dipartimento di Matematica, Università di Pisa, Largo B. Pontecorvo, 5, 56127 Pisa, Italy*

(Dated: October 29, 2024)

We derive asymptotically exact formulas for the equilibrium magnetic stripe period in ultrathin films with out-of-plane anisotropy that include the full domain wall magnetic dipolar energy. Starting with the reduced two-dimensional micromagnetic model valid for thin films, we obtain the leading order approximation for the energy per unit volume in the vanishing film thickness limit in the case of Bloch and Néel wall rotations. Its minimization in the stripe period leads to an analytical expression for the equilibrium period with a prefactor proportional to the Bloch wall width. The constant in the prefactor, related to the long-range dipolar interactions, is carefully evaluated. This results in a remarkable agreement of the stripe domain energy density and stripe period predicted by our analytical formulas with micromagnetic simulations. Our formula can be used to accurately deduce magnetic parameters from the experimental measurements of the stripe period and to systematically predict the equilibrium stripe periods in ultrathin films.

I. INTRODUCTION

Magnetic domain observation and prediction have been the subject of continuous scientific interest for over a hundred years[1]. The characteristics of magnetization patterns are notoriously difficult to elucidate, since they intricately depend on the balance of multiple interactions present in magnetic systems. A particular challenge comes from the fact that magnetic systems fall into the category of systems with competing short-range and long-range interactions[1–3]. Specifically, magnetic stripes and bubbles in ferromagnetic films with out-of-plane anisotropy are a prime example of the magnetic domain patterns forming as a result of such a competition. They were first observed at the end of the 50's and were the subject of extensive studies related to their application in magnetic bubble memories[4,5]. In the late 80's, the progress in deposition techniques enabling atomically resolved growth of ultrathin film multilayers led to a revival in magnetic domain observations in thin films with out-of-plane anisotropy and to the discovery of properties specific to the nanoscale. These lower-dimensional magnetic systems gave rise to multiple new opportunities in both fundamental and applied magnetism[6].

In magnetic thin films the magnetostatic interaction tends to maintain the magnetization in the film plane[7]. However, it was observed that for films of thicknesses of the order of a few nanometers or less, the anisotropy of interfacial origin may promote an out-of-plane magnetization in transition metal systems[8]. Magnetic stripe patterns were observed in multilayers[9–11] and ultrathin films with thicknesses tuned close to the spin reorientation transition[12–14]. More recently, the presence of a Dzyaloshinskii-Moriya interaction (DMI) of interfacial origin in ultrathin films was brought to light[15,16]. Chiral Néel stripes[17] and skyrmionic bubbles[18] were observed in ultrathin films. The possibility to manipulate skyrmions by currents[18] and electric fields[19], and the associated potential of skyrmions for information technology applications[20,21] led to a second revival in experimental and theoretical investigations on magnetic stripes in ultrathin magnetic films and multilayers.

Modeling of magnetization patterns in thin films requires to evaluate precisely the demagnetizing energy, a notoriously difficult task owing to the slow convergence and often singular behavior of the demagnetizing energy integrals in space due to the long-range nature of the magnetostatic interaction. For example, it is not possible to calculate exactly the demagnetizing energy of an isolated 1D domain wall in a film of infinite extent in the plane, as the respective integrals diverge[22]. In the ultrathin film limit, the magnetic surface and volume charges decouple[23] and the full demagnetizing energy including long-range dipolar interaction can be calculated explicitly in the case of a compact magnetic skyrmion, using Fourier transform[24,25]. In the case of stripe domains, the periodic character of the pattern enables the use of Fourier series. This feature resulted in various modeling studies of stripe patterns in a countless number of publications, among which only a few will be cited here.

Theoretical studies of stripes started with the work of Kittel, who treated the case of equilibrium stripe periods much smaller than the film thickness[26]. This was followed by the work of Maleck and Kamberský[27], who studied the case of thicknesses of the order or lower than the domain width and predicted an increase of the stripe period with the decrease of the film thickness under a certain threshold thickness. Kooy and Enz proposed a generalized demagnetizing energy applicable to a wide range of thicknesses[28].

In the case of a magnetic monolayer, Yafet and Gyorgy included explicitly the domain wall dipolar energy and predicted a striped ground state for sufficiently large

anisotropy[29]. Czech and Villain considered a regime in which a monolayer may exhibit an exponential dependence of the domain size on the inverse strength of the dipolar interaction[30], a behavior that was already identified for the stripe patterns in the context of Langmuir monolayers, whose modeling bears many similarities to magnetic systems[31]. Kaplan and Gehring[32] proposed a micromagnetic model in which the domain wall thickness is neglected and obtained a semi-analytical formula predicting a stripe period with an exponential dependence on the inverse film thickness. This formula was later derived explicitly by Millev[33], who obtained an analytical expression for the prefactor under the same assumptions. In parallel, Kashuba and Pokrovsky[34], and later Sukstanskii and Primak[35], took into account the finite domain wall width in an ultrathin film and derived an analytical formula, where the film thickness present in the Kaplan and Gehring formula in the prefactor is replaced by the Bloch wall width.

More recently, studies of the stripe problem took into account the Néel character of the domain wall that results in an additional nonlocal dipolar energy term related to the volume magnetic charges. Lemesh et al.[36] derived an expression for the energy whose numerical minimization gives a prediction of the stripe period, as well as the domain wall width and angle. Meier et al. proposed a modified version of the Kashuba and Pokrovsky formula taking into account the Néel character of the domain wall[37].

Despite the extensive efforts in modeling the stripe patterns in magnetic thin films, at present there exists no clarity about the regime of validity of various existing analytical formulas for the equilibrium stripe periods. Formulas with a prefactor proportional to the film thickness[19,38–43] or the Bloch wall width[37,44–46] are used indiscriminately for ultrathin films, despite presenting up to more than one order of magnitude difference[47]. Additionally, even among the models which take into account the domain wall long-range dipolar contributions in the stripe energy, resulting in an analytical formula with a prefactor proportional to the Bloch wall width[34,35,37,47], there exist discrepancies in the estimated constants in front of the prefactor up to a factor of 3. This is problematic, as these formulas often serve as a tool to quantitatively estimate the domain wall energy from the stripe period.

In the present work we settle this issue by calculating an asymptotically exact analytical formula for the equilibrium magnetic stripe period valid in the ultrathin film regime, were the prefactor is calculated explicitly for the case of both Bloch and Néel domain walls. The validity of the obtained formulas is tested using detailed micromagnetic simulations, in which we compare the energy density scaling with the domain period, as well as the domain period variation with the film thickness for systems with and without DMI. Our results confirm that for ultrathin films the full domain wall contribution to the energy needs to be taken into account, leading to a proportionality of the prefactor to the Bloch wall width and providing a prefactor that is asymptotically exact for vanishing thicknesses.

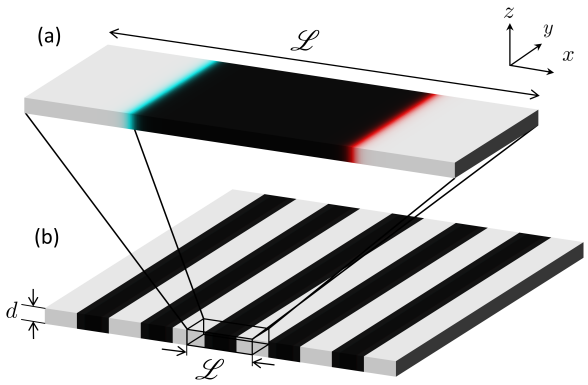

FIG. 1: Schematic representation of an ultrathin film of thickness d with periodic stripe magnetic domains of period $\mathscr{L}$. The black and white colors represent magnetization pointing up and down in the z-direction, while blue and red represent the in-plane magnetization pointing left and right in the x-direction (Néel domain walls).

Our paper is organized as follows. In Sec. II, we present the formulas for the energy per unit volume and the equilibrium period of magnetic stripe domains derived by us, in a dimensional form convenient to use for comparison with experiments. In this section, we also compare the predictions of our formulas with the results of direct numerical simulations for several sets of experimentally relevant parameters and compare our findings with previous literature. The rest of the paper provides the details of our derivation and the simulations. Specifically, in Sec. III, we set up a reduced mathematical model whose solution asymptotically governs the energetics of the equilibrium stripe domains. In Sec. IV, we carry out an asymptotic analysis of this model to extract the leading order expansion for the energy density and the equilibrium stripe period. Finally, in Sec. V we present the details of our numerical simulations and in Sec.VI we draw conclusions.

II. SUMMARY OF THE RESULTS

We consider a sample that consists of a thin ferromagnetic film of thickness d with out-of-plane magnetic anisotropy and infinite extent in the plane. We define the dimensionless film thickness $\delta = d/\ell_{\text{ex}}$, where $\ell_{\text{ex}} = \sqrt{2A_{\text{ex}}/(\mu_0 M_s^2)}$ is the exchange length, A_{ex} the exchange stiffness, μ_0 the vacuum permeability and M_s the saturation magnetization. The film is assumed to be sufficiently thin, $\delta \lesssim 1$, in order for the magnetization vector $\mathbf{M}$ to be independent of the z-variable (see Fig. 1). We introduce the dimensionless DMI strength

$\kappa = D/\sqrt{A_{\rm ex}K_d}$, where $K_d = \frac{1}{2}\mu_0 M_{\rm s}^2$ and D is the interfacial DMI constant (in J/m^2, non-negative without loss of generality). It is widely expected that for δ and κ sufficiently small the magnetic ground state of the sample consists of periodic parallel magnetic stripes with a period $\mathscr{L}$ (see Fig. 1), where the stripes are magnetic domains of width $\simeq \frac{1}{2}\mathscr{L}$ with magnetization pointing alternatively up and down depending only on x, separated by domain walls. We assume that the magnetization vector rotation lies in a plane: either the xz-plane for Néel stripes or the yz-plane for Bloch stripes.

To illustrate our results, we consider the case of a thin transition metal ferromagnetic film with an exchange constant $A_{\rm ex} = 10$ pA/m and saturation magnetization $M_s = 1$ MA/m, resulting in an exchange length $\ell_{\rm ex} \simeq 4$ nm.

A. Bloch stripes

In Sec. IV B, we compute the energy per unit volume $\mathcal{F}(\mathscr{L}) = f(\mathscr{L}/\ell_{\rm ex})K_d$, after subtracting the energy of the uniformly magnetized state, of periodic stripe domains of period $\mathscr{L}$ in the classical case of stripes separated by Bloch walls ($D = 0$). We obtain

$$\mathcal{F}(\mathscr{L}) \simeq \frac{2\sigma_B}{\mathscr{L}} - \frac{4dK_d}{\pi\mathscr{L}}\left[\ln\left(\frac{\mathscr{L}}{\pi^2 L_B}\right) + \gamma + 1\right], \qquad (1)$$

where $\sigma_B = 4\sqrt{A_{\rm ex}K_{\rm eff}}$ is the wall surface tension, in which $K_{\rm eff} = K_u - K_d$ is the effective magnetic anisotropy of the thin film, $L_B = \sqrt{A_{\rm ex}/K_{\rm eff}}$ is the Bloch wall width, and $\gamma \approx 0.5772$ is the Euler-Mascheroni constant. We obtain the leading order optimal period by minimizing $\mathcal{F}(\mathscr{L})$ in $\mathscr{L}$:

$$\mathscr{L}_{\rm opt}^{\rm Bloch} = \pi^2 e^{-\gamma} L_B \exp\left(\frac{\pi\sigma_B}{\mu_0 M_s^2 d}\right). \qquad (2)$$

This formula is asymptotically exact for $d \to 0$.

In order to illustrate the Bloch stripes period formula, we chose a volume magnetocrystalline anisotropy tuned to $K_{u1} = 0.75$ MJ/m^3 (regime 1) and independent of the film thickness (the regime of magnetocrystalline anisotropy of surface origin will be considered in Sec. II B). In Fig. 2, we present the optimal stripe period for regime 1, where the prediction from Eq. (2) is represented as the solid line. We use black dots to present the optimal period obtained using micromagnetic simulations using the MuMax3 software[48]. These numerical results, obtained with the help of the procedure described in detail in Sec. V, were computed by minimizing the energy of one stripe with period $\mathscr{L}$, under periodic boundary conditions (see Fig. 1). The stripe period is varied until the optimal stripe period, corresponding to the smallest minimized energy density, is found. The micromagnetic simulations are in a very good agreement with our asymptotic formula in Eq. (2) for the values of δ up to $\delta = 2$ (see Fig. 2).

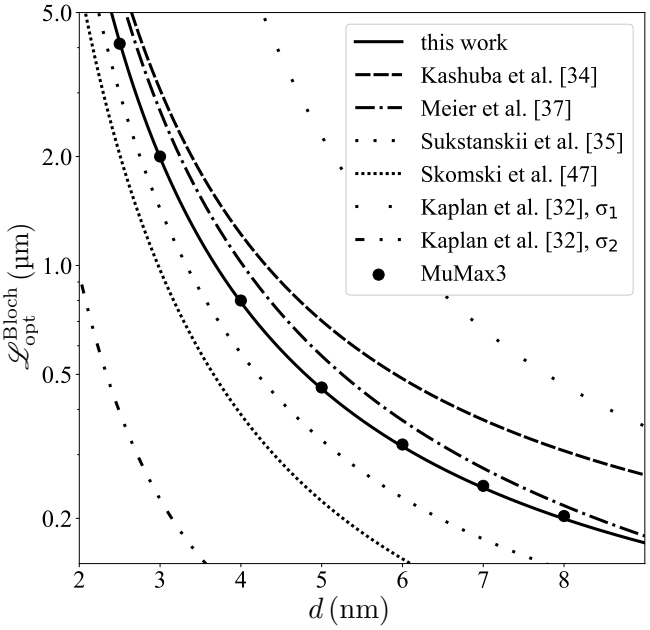

FIG. 2: Equilibrium stripe period $\mathscr{L}_{\rm opt}^{\rm Bloch}$ as a function of the film thickness d in the regime of Bloch walls (zero DMI). The material parameters are $A_{\rm ex} = 10$ pA/m, $M_s = 1$ MA/m and $K_{u1} = 0.75$ MJ/m^3 (regime 1). The asymptotic equilibrium stripe period in Eq. (2) is represented by a solid line. The equilibrium stripe period obtained by micromagnetic simulations using MuMax3[48] (see Sec. V for details) is represented by black dots. The equilibrium stripe periods from previous works[32,34,35,37,47] are also shown (see inset for details).

B. Néel stripes

We now consider a system with DMI, where $\frac{4\ln 2}{\pi^2}dK_d < D < \frac{4}{\pi}\sqrt{A_{\rm ex}K_{\rm eff}}$, i.e., for $D > 0$ sufficiently large to ensure a pure Néel rotation for the wall, but sufficiently small to prevent spin spirals[36,49]. In Sec. IV A, we compute the energy per unit volume $\mathcal{F}(\mathscr{L}) = f(\mathscr{L}/\ell_{\rm ex})K_d$, after subtracting the energy of the uniformly magnetized state, of periodic stripe domains of period $\mathscr{L}$ in the case of Néel walls. We obtain

$$\mathcal{F}(\mathscr{L}) \simeq \frac{2\sigma_N}{\mathscr{L}} - \frac{4dK_d}{\pi\mathscr{L}}\left[\ln\left(\frac{\mathscr{L}}{2\pi^2 L_B}\right) + \gamma + 1\right], \qquad (3)$$

where $\sigma_N = 4\sqrt{A_{\rm ex}K_{\rm eff}} - \pi D > 0$ is the surface tension of the Néel domain wall. Minimizing this energy in $\mathscr{L}$, we obtain

$$\mathscr{L}_{\rm opt}^{\rm Néel} = 2\pi^2 e^{-\gamma} L_B \exp\left(\frac{\pi\sigma_N}{\mu_0 M_s^2 d}\right). \qquad (4)$$

Again, this formula is asymptotically exact for $d \to 0$. This expression differs in two points from that in Eq. (2). First, the expression for the domain wall surface tension appearing in the exponential factor is, as expected, taking into account a decrease in the surface tension by πD due to DMI[49,50]. Second, a factor of two, related

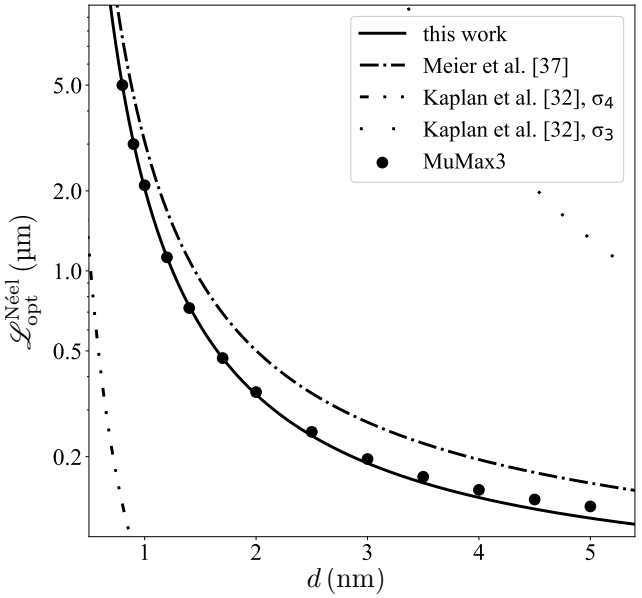

FIG. 3: Equilibrium stripe period $\mathscr{L}_{\mathrm{opt}}^{\mathrm{Néel}}$ as a function of the film thickness d in the case of Néel walls. The thin film parameters are $A_{\mathrm{ex}} = 10$ pA/m, $M_s = 1$ MA/m, $K_{u2} = 1$ MJ/m^3 and $D_2 = 2$ mJ/m^2 (regime 2). The asymptotic equilibrium stripe period in Eq. (4) is represented by a solid line. The equilibrium stripe period obtained by micromagnetic simulations using MuMax3 (see Sec. V for details) and in previous works[32,37] are also presented (see inset for details).

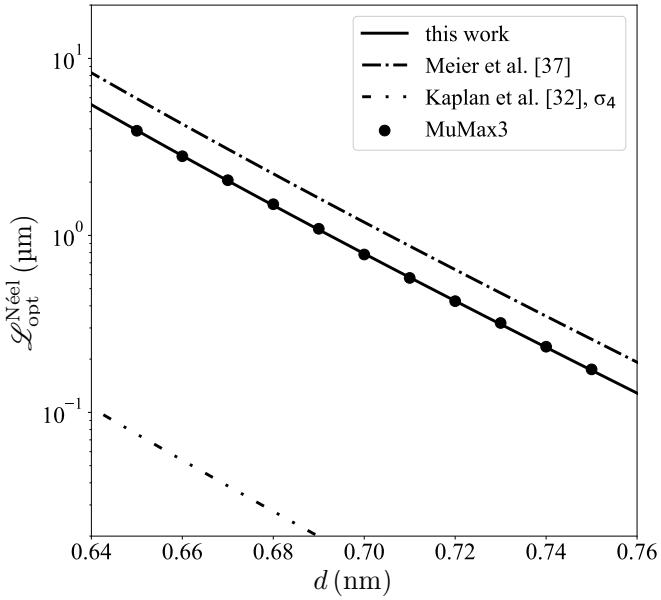

FIG. 4: Equilibrium stripe period $\mathscr{L}_{\mathrm{opt}}^{\mathrm{Néel}}$ as a function of the film thickness d in the case of Néel walls for an ultrathin film with thickness-dependent volume magnetocrystalline anisotropy $K_{u3} = K_{s3}/d$ and thickness-dependent volume DMI $D_3 = D_{s3}/d$. The thin film parameters are $A_{\mathrm{ex}} = 10$ pA/m, $M_s = 1$ MA/m, $K_{s3} = 0.6$ mJ/m^2, and $D_{s3} = 1.2$ pJ/m (regime 3). The asymptotic equilibrium stripe period in Eq. (4) is represented by a solid line. The equilibrium stripe period obtained by micromagnetic simulations using MuMax3[48] (see Sec. V for details) and in previous works[32,37] are also presented (see inset for details).

to the nonlocal dipolar interactions is appearing in the expression for the prefactor in the case of Néel walls. This additional energy is a consequence of the volume charges present in the Néel wall, associated with the in-plane component of the demagnetizing field, whose analytical expression in the limit $d \to 0$ is a well-known result[37,49,51].

The equilibrium stripe period formula for the case of Néel walls in Eq. (4) is illustrated by the solid line in Fig. 3. We present the case of a magnetic thin film with a volume magnetocrystalline anisotropy $K_{u2} = 1$ MJ/m^3 and a volume DMI $D_2 = 2$ mJ/m^2 (regime 2). Our asymptotic formula shows a very good agreement with the micromagnetic simulations for low d and starts to deviate as the thickness becomes greater than the Bloch wall width $d > L_B \simeq 5$ nm, which is outside the range of validity of our expression for the stray field energies valid in the ultrathin film limit[23,50]. Finally, we address the classical regime of a few monolayer transition metal wedge with magnetocrystalline anisotropy and DMI of interfacial origin that are inversely proportional to the film thickness: $K_{u3} = K_{s3}/d$ and $D_3 = D_{s3}/d$ (regime 3)[52]. In this type of systems, the observable stripe domains are present in a very narrow range of thicknesses[12–14,19] (a fraction of a monolayer), as can be seen in Fig. 4. As expected, the asymptotic model is very accurate in this regime, in which $\delta \sim 0.1$.

C. Comparison with previous studies

In Figs. 2–4, we also present the equilibrium stripe periods predicted by existing formulas in the literature and compare them with our asymptotic predictions in Eqs. (2) and (4). We start with the Kaplan and Gehring formula that reads[32,33]

$$\mathscr{L}_{\mathrm{opt}}^{\mathrm{KG}} = \frac{\pi}{\sqrt{e}}\, d \exp\left(\frac{\pi\sigma}{\mu_0 M_s^2 d}\right), \tag{5}$$

where σ is the domain wall surface tension in three dimensions. This formula has been widely used to obtain quantitative information based on experimental measurement of the stripe period in ultrathin films[19,38–43]. However, this formula is valid for films of thicknesses much larger than the Bloch wall width, $d \gg L_B$, which is very unlikely to be the case for an ultrathin film. Notice that if one were to use this formula in the case of the Bloch stripes (no DMI), one would have to choose $\sigma = \sigma_1 = 4\sqrt{A_{\mathrm{ex}} K_u}$, as the corresponding expression for the energy density already takes into account the exact full magnetostatic energy of the three-dimensional magnetic domains with zero wall thickness. Nevertheless, in the literature one often assumed $\sigma = \sigma_2 = 4\sqrt{A_{\mathrm{ex}}(K_u - K_d)}$, which is not consistent with the three-dimensional stray field en-

ergy calculation used. For Néel stripes (with DMI), the correct choice of the domain wall surface tension would be $\sigma = \sigma_3 = 4\sqrt{A_{\rm ex}(K_u + K_d)} - \pi D$ in order to account for the additional stray field energy contribution localized in the one-dimensional wall profile[53]. Nevertheless, $\sigma = \sigma_4 = 4\sqrt{A_{\rm ex}(K_u - K_d)} - \pi D$ has been frequently used. Regardless of the choice of σ, the formula also suffers from the prefactor proportional to the film thickness d. In all the cases, the Kaplan and Gehring formula presents, from one order of magnitude (regime 1, see Fig. 2), up to two orders of magnitude (regimes 2 and 3, see Figs. 3 and 4) errors in the predicted equilibrium stripe period compared to our asymptotic formula, and its use should, therefore, be avoided in the case of ultrathin films with $d \lesssim L_B$.

The formulas of Kashuba and Pokrovsky[34], Sukstanskii and Primak[35], and Skomski et. al[47] are, on the contrary, valid in the ultrathin film limit, i.e., for $d \lesssim L_B$. They are represented for the Bloch case in Fig. 2. They differ from Eq. (2) only by the numerical constant in front of the Bloch wall width in the prefactor, since their prefactor is proportional to the Bloch wall width as in Eq. (2). This constant is resulting from the long-range dipolar interaction energy term for the stripe system, which is calculated by evaluating a series (see Sec. IV). Different assumptions or incorrect evaluation of these series led to different prefactor constants in those previous studies and to under- or overestimation of the equilibrium stripe periods of less than an order of magnitude (see Fig. 2).

Finally, we compare our result with the work of Meier et al.[37]. In their work, Meier et al. used the expression given by Kashuba and Pokrovsky[34] for the long-range dipolar interaction energy of the stripe domains. They introduced three modifications as compared to Kashuba and Pokrovsky. First, the expression of the domain wall surface tension appearing in the exponential factor is modified to account for the wall surface tension decrease by πD in presence of DMI[49], in agreement with Eq. (4). Second, they account for the increase in the wall surface tension as the result of the presence of volume charges in the case of a Néel wall[51]. This leads to an additional factor of two in their prefactor as compared to the Bloch case in agreement with the additional factor of 2 in Eq. (4) as compared to Eq. (2). Third, they introduce a thickness-dependent domain wall width and domain wall surface tension. One can see in Fig. 2 that this last modification introduced by Meier et al. leads to a slight decrease of the predicted stripe period compared to that of Kashuba and Pokrovsky in the case of the Bloch stripes and a slight apparent improvement of the agreement with the numerics. Nevertheless, this improvement is somewhat fortuitous, since the asymptotic behavior of the formula of Meier et al. is the same as that of Kashuba and Pokrovsky, which presents around a 50% discrepancy with our exact asymptotic formula and the results of direct numerical minimization of the micromagnetic energy (see also Figs. 3 and 4 for the case of the Néel stripes). Our asymptotic formula, on the other hand, yields a very good accuracy throughout the entire thickness range as long as the film thickness is lower than the Bloch width without the need to introduce any further thickness dependence related to wall surface tension or domain wall width thickness variation (see Figs. 2–4, see also sec. V for a discussion on the domain wall width thickness variation).

III. MODEL

We now present a detailed derivation of our formulas. We begin by specifying the microscopic sample geometry. For simplicity, we consider an extended material in the film plane and impose periodic boundary conditions to avoid the need to deal with the material edge effects (the treatment of the latter in the case of ultra-thin films can be found in[54]). Let $\mathbb{T}^2_{\mathscr{L}} = [0, \mathscr{L})^2$ be a flat two-dimensional torus (a square box of sidelength $\mathscr{L}$ with periodic boundary conditions) with $\mathscr{L}$ macroscopically large. For a single layer of total thickness d we define $\widetilde{\Omega} = \mathbb{T}^2_{\mathscr{L}} \times (-d/2, d/2) \subset \mathbb{R}^3$ to be the set occupied by the ferromagnetic layer. Next we write the full micromagnetic energy functional (in the SI units) for three-dimensional configurations $\mathbf{M} = \mathbf{M}(x, y, z)$ described by the magnetization vector $\mathbf{M} : \mathbb{T}^2_{\mathscr{L}} \times \mathbb{R} \to \mathbb{R}^3$ satisfying $|\mathbf{M}| = M_s$, the saturation magnetization (in A/m), in $\widetilde{\Omega}$, and $\mathbf{M} = 0$ outside $\widetilde{\Omega}$, with no applied field[2,49]:

$$\begin{aligned}\mathcal{E}^{3d}(\mathbf{M}) = &\int_{\widetilde{\Omega}} \left(\frac{A_{\rm ex}}{M_s^2} |\nabla \mathbf{M}|^2 + \frac{K_u}{M_s^2} |\mathbf{M}_\perp|^2 \right) d^3 r \\ &+ \frac{D}{M_s^2} \int_{\widetilde{\Omega}} \left(M_\parallel \nabla_\perp \cdot \mathbf{M}_\perp - \mathbf{M}_\perp \cdot \nabla_\perp M_\parallel \right) d^3 r \\ &- \frac{\mu_0}{2} \int_{\widetilde{\Omega}} \mathbf{H}_d \cdot \mathbf{M} \, d^3 r - \frac{1}{2} \mu_0 M_s^2 \mathscr{L}^2 d,\end{aligned} \tag{6}$$

where we used the notation $\mathbf{M} = (\mathbf{M}_\perp, M_\parallel) \in \mathbb{R}^3$ with $\mathbf{M}_\perp \in \mathbb{R}^2$ denoting the in-plane component of $\mathbf{M}$ and $M_\parallel \in \mathbb{R}$ denoting the out-of-plane component of $\mathbf{M}$ (parallel to the out-of-plane easy axis); the operator $\nabla_\perp = (\partial_x, \partial_y)$ denotes the in-plane portion of the gradient. The terms in the energy are, in order of appearance: the exchange and the crystalline anisotropy with exchange stiffness $A_{\rm ex}$ (in J/m, positive) and uniaxial perpendicular anisotropy constant K_u (in J/m^3, positive), respectively; the interfacial DMI constant D (in J/m^2, of arbitrary sign); the stray field energy with the vacuum permeability μ_0 and $\mathbf{H}_d$ being the demagnetizing field solving the static Maxwell's equations distributionally in $\mathbb{T}^2_{\mathscr{L}} \times \mathbb{R}$:

$$\nabla \cdot (\mathbf{H}_d + \mathbf{M}) = 0, \qquad \nabla \times \mathbf{H}_d = 0, \tag{7}$$

with periodic boundary conditions in the plane and vanishing as $z \to \pm\infty$; and an additive constant chosen so that $\mathcal{E}^{3d}(\mathbf{M}) = 0$ for $\mathbf{M} = \pm M_s \chi_{\widetilde{\Omega}} \hat{\mathbf{z}}$, where $\chi_{\widetilde{\Omega}}$ is the characteristic function of $\widetilde{\Omega}$, i.e., to offset the energy of the monodomain state.

We next carry out a suitable non-dimensionalization. We measure all lengths in the units of the exchange length $\ell_{\rm ex} = \sqrt{2A_{\rm ex}/(\mu_0 M_s^2)}$ and define the normalized magnetization and energy

$$\mathbf{m} = \frac{\mathbf{M}}{M_s}, \qquad E^{3d} = \frac{\mathcal{E}^{3d}}{A_{\rm ex} d}. \tag{8}$$

Then the rescaled micromagnetic energy E^{3d} is a function of $\mathbf{m} : \mathbb{T}^2_L \times \mathbb{R} \to \mathbb{R}^3$ with $|\mathbf{m}| = 1$ in $\Omega = \mathbb{T}^2_L \times (-\delta/2, \delta/2)$ and $|\mathbf{m}| = 0$ in the complement of Ω, where

$$L = \frac{\mathscr{L}}{\ell_{\rm ex}}, \qquad \delta = \frac{d}{\ell_{\rm ex}}, \tag{9}$$

and may be written as

$$\begin{aligned} E^{3d}(\mathbf{m}) = {} & \frac{1}{\delta} \int_\Omega \left(|\nabla \mathbf{m}|^2 + Q |\mathbf{m}_\perp|^2 - 1 \right) d^3 r \\ & + \frac{\kappa}{\delta} \int_\Omega \left(m_\parallel \nabla_\perp \cdot \mathbf{m}_\perp - \mathbf{m}_\perp \cdot \nabla_\perp m_\parallel \right) d^3 r \\ & + \frac{1}{\delta} \int_{\mathbb{T}^2_L \times \mathbb{R}} \nabla \cdot \mathbf{m} (-\Delta)^{-1} \nabla \cdot \mathbf{m} \, d^3 r. \end{aligned} \tag{10}$$

Here we introduced the dimensionless effective material quality factor Q and the dimensionless DMI strength κ:

$$Q = \frac{2K_u}{\mu_0 M_s^2}, \qquad \kappa = D \sqrt{\frac{2}{\mu_0 M_s^2 A_{\rm ex}}}, \tag{11}$$

as well as the inverse Laplacian operator $(-\Delta)^{-1}$ whose action on three-dimensional plane waves is defined as

$$e^{-i\mathbf{k}\cdot\mathbf{r}} (-\Delta)^{-1} e^{i\mathbf{k}\cdot\mathbf{r}} = \frac{1}{|\mathbf{k}|^2}, \tag{12}$$

expressing the fact that the stray field energy represents the Coulombic repulsive energy of the "magnetic charges", whose density $\rho = -\nabla \cdot \mathbf{m}$ is understood in the distributional sense in $\mathbb{T}^2_L \times \mathbb{R}$ (Ref.[55]). In the rest of the paper we always consider the non-dimensional version of the problem. For definiteness we also assume from now on that $\kappa \geq 0$, without loss of generality.

We now introduce a reduced two-dimensional micromagnetic model appropriate for ultra-thin films corresponding to $\delta \ll 1$. We define the magnetization $\mathbf{m} = \mathbf{m}(x, y)$ on a flat torus $\mathbb{T}^2_L = [0, L)^2$. The non-dimensional energy of such a configuration in Ω is obtained via a suitable asymptotic reduction from Eq. (10) in the ultra-thin film limit (for $\delta \ll 1$) and, up to an additive constant, reads[23,50]

$$\begin{aligned} E^{2d}_L(\mathbf{m}) = {} & \int_{\mathbb{T}^2_L} \left(|\nabla \mathbf{m}|^2 + (Q-1) |\mathbf{m}_\perp|^2 \right) d^2 r \\ & + \kappa \int_{\mathbb{T}^2_L} \left(m_\parallel \nabla \cdot \mathbf{m}_\perp - \mathbf{m}_\perp \cdot \nabla m_\parallel \right) d^2 r \\ & - \frac{\delta}{2} \int_{\mathbb{T}^2_L} m_\parallel (-\Delta)^{1/2} m_\parallel \, d^2 r \\ & + \frac{\delta}{2} \int_{\mathbb{T}^2_L} \nabla \cdot \mathbf{m}_\perp (-\Delta)^{-1/2} \nabla \cdot \mathbf{m}_\perp \, d^2 r. \end{aligned} \tag{13}$$

Here the symbols $(-\Delta)^{1/2}$ and $(-\Delta)^{-1/2}$ denote the half-Laplacian operator and its inverse, respectively, whose actions on two-dimensional plane waves are defined as

$$e^{-i\mathbf{k}\cdot\mathbf{r}} (-\Delta)^{1/2} e^{i\mathbf{k}\cdot\mathbf{r}} = |\mathbf{k}|, \tag{14}$$

$$e^{-i\mathbf{k}\cdot\mathbf{r}} (-\Delta)^{-1/2} e^{i\mathbf{k}\cdot\mathbf{r}} = \frac{1}{|\mathbf{k}|}. \tag{15}$$

The terms associated with the half-Laplacian describe the nonlocal contributions of the stray field due to the surface and volume charges, respectively, with the usual local surface charge contribution renormalizing the out-of-plane anisotropy constant. In particular, we have $E^{2d}_L(\mathbf{m}) \simeq E^{3d}(\mathbf{m}\chi_\Omega)$ for $\delta \ll 1$, where χ_Ω is the characteristic function of the set Ω and $\mathbf{m}\chi_\Omega$ represents a three-dimensional magnetization configuration in the film that does not vary along the z-direction.

A. Néel stripes

It may be conjectured, although it is a very difficult and unsolved mathematical problem, that the global energy minimizer of this energy with κ and δ small, and with L sufficiently large, is given by a periodic array of stripes in which the magnetization rotates between the two easy directions $\pm\hat{\mathbf{z}}$. In the presence of interfacial DMI the rotation of the magnetization vector in the domain walls changes its character from Bloch to Néel. Hence, assuming that the magnetization profile is a one-dimensional Néel rotation with angle $\theta = \theta(x)$, i.e., that

$$\mathbf{m} = (\sin\theta(x), 0, \cos\theta(x)), \tag{16}$$

the energy of such a configuration is $E^{2d}_L(\mathbf{m}) = L E^{1d}_L(\theta)$, where

$$\begin{aligned} E^{1d}_L(\theta) = {} & \int_0^L \left(|\theta'|^2 + (Q-1) \sin^2\theta + \kappa\theta' \right) dx \\ & - \frac{\delta}{2} \int_0^L \cos\theta \left(-\frac{d^2}{dx^2} \right)^{1/2} \cos\theta \, dx \\ & + \frac{\delta}{2} \int_0^L \sin\theta \left(-\frac{d^2}{dx^2} \right)^{1/2} \sin\theta \, dx, \end{aligned} \tag{17}$$

where the fractional operator $\left(-\frac{d^2}{dx^2} \right)^{1/2}$ is the one-dimensional version of half-Laplacian, whose action on one-dimensional plane waves is defined as

$$e^{-ikx} \left(-\frac{d^2}{dx^2} \right)^{1/2} e^{ikx} = |k|. \tag{18}$$

Note that this operator admits the following integral representation[56,57]:

$$\left(-\frac{d^2}{dx^2} \right)^{1/2} u(x) = \frac{1}{\pi} \, \text{p.v.} \int_{-\infty}^{\infty} \frac{u(x) - u(x')}{|x - x'|^2} \, dx', \tag{19}$$

where p.v. denotes the principal value of the integral at $x' = x$, for any smooth periodic function u defined on the whole real line.

The optimal configuration is obtained by minimizing the energy E_L^{2d} per unit area, hence if θ_L is a minimizer of E_L^{1d} and the stripe conjecture is valid, we have

$$f(L) = \frac{1}{L} E_L^{1d}(\theta_L) = \min_{\mathbf{m} \in H^1(\mathbb{T}_L^2; \mathbb{S}^2)} \frac{1}{L^2} E_L^{2d}(\mathbf{m}), \tag{20}$$

where the latter minimization is carried out over the standard class $H^1(\mathbb{T}_L^2; \mathbb{S}^2)$ of three-dimensional vector fields with values on a unit sphere and with square integrable weak derivatives. A posteriori, any minimizer is known to be smooth and to satisfy the Euler-Lagrange equation

$$\begin{aligned} 0 = \theta_L''(x) - &(Q-1)\sin\theta_L(x)\cos\theta_L(x) \\ &- h_s(x)\sin\theta_L(x) + h_v(x)\cos\theta_L(x), \end{aligned} \tag{21}$$

where the effective fields h_s and h_v due to the long-range dipolar contributions of the surface and volume charges are, respectively,

$$h_s = \frac{\delta}{2}\left(-\frac{d^2}{dx^2}\right)^{1/2} \cos\theta_L, \tag{22}$$

$$h_v = -\frac{\delta}{2}\left(-\frac{d^2}{dx^2}\right)^{1/2} \sin\theta_L, \tag{23}$$

and the energy density $f(L)$ may be alternatively written as

$$\begin{aligned} f(L) = -\frac{2\pi\kappa}{L} + \frac{1}{L}\int_0^L &(|\theta_L'|^2 + (Q-1)\sin^2\theta_L \\ &- h_v \sin\theta_L - h_s\cos\theta_L) dx. \end{aligned} \tag{24}$$

As $\cos\theta_L$ and $\sin\theta_L$ are assumed to be periodic, without loss of generality one can take L to be the fundamental period of the stripes, which we do from now on. The DMI term forces winding of the angle by -2π over the fundamental period for $\kappa > 0$, hence after a suitable translation we may assume that $\theta_L(x)$ decreases from $\theta_L(0) = \frac{\pi}{2}$ to $\theta_L(L) = -\frac{3\pi}{2}$. Thus Eq. (21) should be solved on the interval $(0, L)$ with the above Dirichlet boundary conditions at $x = 0$ and $x = L$. Furthermore, as there is no applied magnetic field, we may assume an additional symmetry $\theta_L(\frac{L}{2}+x) = \theta_L(x) - \pi$ for $x \in (0, \frac{L}{2})$, consistent with Eq. (21), which allows to restrict the solution of Eq. (21) to the interval $(0, \frac{L}{2})$ with Dirichlet boundary conditions $\theta_L(0) = \frac{\pi}{2}$ and $\theta_L\left(\frac{L}{2}\right) = -\frac{\pi}{2}$. In fact, one further expects that θ_L is an odd function around $x = \frac{L}{4}$ on $\left(0, \frac{L}{2}\right)$, i.e., $\theta_L(x) = -\theta_L\left(\frac{L}{2} - x\right)$. In particular, $\theta_L(x)$ decreases from $\theta_L(0) = \frac{\pi}{2}$ to $\theta_L\left(\frac{L}{4}\right) = 0$ on $\left(0, \frac{L}{4}\right)$. Notice that these assumptions are consistent with Eq. (21), since $\cos\theta_L$ and $\sin\theta_L$ being an even and odd function on $\left(0, \frac{L}{2}\right)$ around the midpoint $x = \frac{L}{4}$ results in h_s and h_v also being an even and odd functions, respectively, consistent with θ_L'' being an odd function.

B. Bloch stripes

Here we briefly adapt the calculation above to the case of $\kappa = 0$, no DMI. In this case the optimal stripe profile is of Bloch type:

$$\mathbf{m} = (0, \sin\theta(x), \cos\theta(x)), \tag{25}$$

in order to minimize the contribution of bulk charges to the stray field energy. As there is no contribution from bulk charges in this case, the energy is

$$\begin{aligned} E_L^{1d}(\theta) = &\int_0^L (|\theta'|^2 + (Q-1)\sin^2\theta) dx \\ &- \frac{\delta}{2}\int_0^L \cos\theta \left(-\frac{d^2}{dx^2}\right)^{1/2} \cos\theta \, dx, \end{aligned} \tag{26}$$

and the Euler-Lagrange equation satisfied by an associated minimizer θ_L is

$$\begin{aligned} 0 = \theta_L''(x) - &(Q-1)\sin\theta_L(x)\cos\theta_L(x) \\ &- h_s(x)\sin\theta_L(x). \end{aligned} \tag{27}$$

Contrary to the case of strong DMI, with only the surface charge contribution to the energy present the optimal profile $\theta_L(x)$ is expected to exhibit no winding and hence be periodic (see also[58]). The energy density of stripes is then given by

$$f(L) = \frac{1}{L}\int_0^L \left(|\theta_L'|^2 + (Q-1)\sin^2\theta_L - h_s\cos\theta_L\right) dx. \tag{28}$$

IV. CALCULATION OF THE OPTIMAL STRIPE PERIOD IN ULTRATHIN FILMS

We now investigate the minimization problem associated with $f(L)$ in the limit $\delta \to 0$. It is known rigorously[23] that in this regime (with the effect of not too strong DMI readily incorporated as in[50]) the average length scale of the energy-minimizing patterns for Eq. (13) on all sufficiently large spatial domains scales as

$$L \sim \frac{e^{a/\delta}}{\sqrt{Q-1}}, \qquad a = \frac{\pi}{2}\left(4\sqrt{Q-1} - \pi\kappa\right) > 0. \tag{29}$$

In particular, under the periodic stripe conjecture Eq. (29) gives the leading order scaling (up to a prefactor) of the optimal stripe period. Furthermore, if L is the fundamental period, we have $\left|E_L^{1d}(\theta_L)\right| \le C$ for some constant $C > 0$ independent of δ, and the same estimate holds for every term in the energy separately[23].

A. Néel stripes period

To calculate the optimal period, we first need to approximate the energy density $f(L)$ for sufficiently small

values of δ. This requires to find a leading order approximation to the minimizing profile θ_L, which in view of the fact that $L \to \infty$ as $\delta \to 0$ is, in principle, a singular perturbation problem. Nevertheless, at least formally it is possible to show that the leading order behavior of θ_L on the interval $\left(0, \frac{L}{4}\right)$ may be obtained by setting $\delta = 0$ in Eq. (21), yielding a unique monotonically decreasing solution $\theta_L^{(0)}$ satisfying $\theta_L^{(0)}(0) = \frac{\pi}{2}$ and $\theta_L^{(0)}\left(\frac{L}{4}\right) = 0$. Indeed, from the integral representation of $\left(-\frac{d^2}{dx^2}\right)^{1/2}$ in Eq. (19) we have for any function $u \in C^\infty(\mathbb{R}) \cap L^\infty(\mathbb{R})$

$$\begin{aligned}\left(-\frac{d^2}{dx^2}\right)^{1/2} u(x) &= \frac{1}{\pi}\,\text{p.v.}\int_{x-1}^{x+1} \frac{u(x)-u(x')}{|x-x'|^2}\,dx' \\ &+\frac{1}{\pi}\int_{-\infty}^{x-1} \frac{u(x)-u(x')}{|x-x'|^2}\,dx' + \frac{1}{\pi}\int_{x+1}^{\infty} \frac{u(x)-u(x')}{|x-x'|^2}\,dx'.\end{aligned} \tag{30}$$

Therefore

$$\left\|\left(-\frac{d^2}{dx^2}\right)^{1/2} u\right\|_{L^\infty(\mathbb{R})} \le \frac{4}{\pi}\|u\|_{L^\infty(\mathbb{R})} + \frac{1}{\pi}\|u''\|_{L^\infty(\mathbb{R})}. \tag{31}$$

Thus, with $u = \cos\theta_L$ or $u = \sin\theta_L$ we have

$$\begin{aligned}&\|h_s\|_{L^\infty(\mathbb{R})} + \|h_v\|_{L^\infty(\mathbb{R})} \\ &\quad\le C\delta\left(1 + \|\theta_L'\|_{L^\infty(\mathbb{R})}^2 + \|\theta_L''\|_{L^\infty(\mathbb{R})}\right),\end{aligned} \tag{32}$$

for some universal constant $C > 0$. Furthermore, arguing as in[59], one can show that $\|\theta_L'\|_{L^\infty(\mathbb{R})}$ and $\|\theta_L''\|_{L^\infty(\mathbb{R})}$ are both uniformly bounded for all bounded solutions of Eq. (21), hence the stray field terms are uniformly small, and one can therefore look for a solution of the Dirichlet problem for Eq. (21) in the form of a regular series expansion in δ. Furthermore, it is not difficult to see directly from Eq. (21) with $\delta = 0$ that

$$\theta_L^{(0)}(x) = \arccos\left[\tanh\left(x\sqrt{Q-1}\right)\right] + O(e^{-cL}), \tag{33}$$

for some $c > 0$ when $L \gg 1$, for all $x \in \left(0, \frac{L}{4}\right)$.

Having formally established that the minimizer $\theta_L \simeq \theta_L^{(0)}$ to within $O(\delta)$ accuracy, we proceed to calculate to the leading order in δ:

$$\begin{aligned}f(L) &= -\frac{2\pi\kappa}{L} \\ &+ \frac{4}{L}\int_0^{L/4}\left(\left|\frac{d\theta_L^{(0)}}{dx}\right|^2 + (Q-1)\sin^2\theta_L^{(0)}\right)dx \\ &+ \frac{2\delta}{L}\int_0^{L/4}\left(\sin\theta_L^{(0)}\left(-\frac{d^2}{dx^2}\right)^{1/2}\sin\theta_L^{(0)}\right)dx \\ &- \frac{2\delta}{L}\int_0^{L/4}\left(\cos\theta_L^{(0)}\left(-\frac{d^2}{dx^2}\right)^{1/2}\cos\theta_L^{(0)}\right)dx \\ &+ \frac{O(\delta^2)}{L},\end{aligned} \tag{34}$$

where the $O(\delta^2)$ error term arises from the fact that $\theta_L^{(0)}$ is a strict local minimizer of E_L^{1d} with $\delta = 0$ and the same boundary data, and that $\theta_L - \theta_L^{(0)} = O(\delta)$. Furthermore, as the perturbations are localized in the vicinity of the domain walls, this error term is expected to be uniform in L. Indeed, with the minimizer θ_L close to $\theta_L^{(0)}$, by Eq. (19) we have

$$h_s(x) \sim \frac{\delta}{x}, \qquad h_v(x) \sim \frac{\delta}{x^2}, \qquad 1 \ll x \ll L. \tag{35}$$

Hence the perturbation effectively vanishes in the space between the domain walls.

We now write $f(L) \simeq f_1(L) + f_2(L)$, where f_1 is the sum of the first and the second lines, and f_2 is the sum of the third and the fourth lines in the right-hand side of Eq. (34). An explicit calculation shows that

$$f_1(L) = \frac{2}{L}\left(4\sqrt{Q-1} - \pi\kappa\right) + O\left(e^{-cL}\right), \tag{36}$$

for some $c > 0$ and all $\delta \ll 1$. This is just the energy of two Néel walls per period, up to the exponential order in $L \gg 1$.

To calculate f_2, we pass to the Fourier series representations of $\cos\theta_L^{(0)}$ and $\sin\theta_L^{(0)}$. From the symmetries of $\theta_L^{(0)}$ we have $\cos\theta_L^{(0)}(x) = \cos\theta_L^{(0)}\left(\frac{L}{2} - x\right)$ and $\sin\theta_L^{(0)}(x) = -\sin\theta_L^{(0)}\left(\frac{L}{2} - x\right)$ for $x \in [\frac{L}{4}, \frac{L}{2}]$, and $\cos\theta_L^{(0)}(x) = -\cos\theta_L^{(0)}(L-x)$ and $\sin\theta_L^{(0)}(x) = \sin\theta_L^{(0)}(L-x)$ for $x \in [\frac{L}{2}, L]$. Defining the Fourier series of the resulting functions, we then obtain

$$\sin\theta_L^{(0)}(x) = \sum_{m=1}^{\infty} a_{2m-1}\cos\left(\frac{2\pi(2m-1)x}{L}\right), \tag{37}$$

$$\cos\theta_L^{(0)}(x) = \sum_{m=1}^{\infty} b_{2m-1}\sin\left(\frac{2\pi(2m-1)x}{L}\right). \tag{38}$$

Using the fact that by Eq. (33) we have

$$\cos\theta_L^{(0)}(x) \simeq \tanh\left(x\sqrt{Q-1}\right), \qquad x \in \left[0, \tfrac{L}{4}\right], \tag{39}$$

$$\sin\theta_L^{(0)}(x) \simeq \operatorname{sech}\left(x\sqrt{Q-1}\right), \qquad x \in \left[0, \tfrac{L}{4}\right], \tag{40}$$

up to $O(e^{-cL})$ errors, the coefficients of the sine series

can be computed as

$$\begin{aligned} b_{2m-1} &= \frac{4}{L}\int_0^{L/2} \cos\theta_L^{(0)}(x)\sin\left(\frac{2\pi(2m-1)x}{L}\right)dx \\ &= -\frac{2}{(2m-1)\pi} \\ &\times \int_0^{L/2} \frac{d\theta_L^{(0)}(x)}{dx}\sin\theta_L^{(0)}(x)\cos\left(\frac{2\pi(2m-1)x}{L}\right)dx \\ &= -\frac{4}{(2m-1)\pi} \\ &\times \int_0^{L/4} \frac{d\theta_L^{(0)}(x)}{dx}\sin\theta_L^{(0)}(x)\cos\left(\frac{2\pi(2m-1)x}{L}\right)dx \\ &\simeq \frac{4\sqrt{Q-1}}{(2m-1)\pi} \\ &\times \int_0^{\infty} \mathrm{sech}^2\left(x\sqrt{Q-1}\right)\cos\left(\frac{2\pi(2m-1)x}{L}\right)dx \\ &= \frac{4\pi}{L\sqrt{Q-1}}\,\mathrm{csch}\left(\frac{(2m-1)\pi^2}{L\sqrt{Q-1}}\right), \end{aligned} \tag{41}$$

where we integrated by parts in the first line and used the symmetry of $\cos\theta_L^{(0)}$ in the second line, again with errors of exponential order. Similarly, the coefficients of the cosine series are

$$\begin{aligned} a_{2m-1} &= \frac{8}{L}\int_0^{L/4} \sin\theta_L^{(0)}(x)\cos\left(\frac{2\pi(2m-1)x}{L}\right)dx \\ &\simeq \frac{8}{L}\int_0^{\infty} \mathrm{sech}\left(x\sqrt{Q-1}\right)\cos\left(\frac{2\pi(2m-1)x}{L}\right)dx \\ &= \frac{4\pi}{L\sqrt{Q-1}}\,\mathrm{sech}\left(\frac{(2m-1)\pi^2}{L\sqrt{Q-1}}\right). \end{aligned} \tag{42}$$

Finally, with the help of Eq. (18) and Eq. (34) the stray field energy density is

$$\begin{aligned} f_2(L) &\simeq -\frac{\pi\delta}{2L}\sum_{m=1}^{\infty}(2m-1)\left(|b_{2m-1}|^2-|a_{2m-1}|^2\right) \\ &= -\frac{32\pi^3\delta}{L^3(Q-1)} \\ &\times \sum_{m=1}^{\infty}(2m-1)\mathrm{csch}^2\left(\frac{2\pi^2(2m-1)}{L\sqrt{Q-1}}\right). \end{aligned} \tag{43}$$

Let us define $s=\frac{2\pi^2}{L\sqrt{Q-1}}$ and compute the above sum as

$$\begin{aligned} &\sum_{m=1}^{\infty}\frac{2m-1}{\sinh^2[(2m-1)s]} \\ &= \sum_{m=1}^{\infty}\frac{m}{\sinh^2(ms)} - \sum_{m=1}^{\infty}\frac{2m}{\sinh^2(2ms)}, \end{aligned} \tag{44}$$

by splitting the series in the first term in the right-hand side into the even and odd terms. Since for $s>0$ the series above converge exponentially fast, we have

$$\begin{aligned} \sum_{m=1}^{\infty}\frac{2m-1}{\sinh^2[(2m-1)s]} &= \frac{d}{ds}\sum_{m=1}^{\infty}(1-\coth(ms)) \\ &- \frac{d}{ds}\sum_{m=1}^{\infty}(1-\coth(2ms)). \end{aligned} \tag{45}$$

Hence it is enough to compute the series

$$\begin{aligned} &\sum_{m=1}^{\infty}(1-\coth(ms)) \\ &= 2\sum_{m=1}^{\infty}\frac{e^{-2ms}}{e^{-2ms}-1} = -2\mathcal{L}(e^{-2s}), \end{aligned} \tag{46}$$

where $\mathcal{L}(q)=\sum_{m=1}^{\infty}\frac{q^m}{1-q^m}$ is a well-studied Lambert series (see e.g.[60]). We obtain

$$\begin{aligned} &\sum_{m=1}^{\infty}\frac{2m-1}{\sinh^2[(2m-1)s]} \\ &= -2\frac{d}{ds}(\mathcal{L}(e^{-2s})-\mathcal{L}(e^{-4s})). \end{aligned} \tag{47}$$

When $s\to 0$ and, hence, $q=e^{-2s}\to 1^-$, we have the following asymptotic expansion of $\mathcal{L}(q)$ (see e.g.[60] (Theorem 2.2(2)), and[61]):

$$\begin{aligned} \mathcal{L}(q) &= \sum_{m=1}^{\infty}\frac{q^m}{1-q^m} \\ &= -\frac{\ln\ln\frac{1}{q}-\gamma}{\ln\frac{1}{q}} + \frac{1}{4} - \sum_{n=1}^{\infty}\frac{B_n^2}{n\,n!}\left(\ln\frac{1}{q}\right)^n, \end{aligned} \tag{48}$$

where γ is the Euler-Mascheroni constant and B_n is the n-th Bernoulli number. Therefore, for $s\to 0$, using Eqs. (47) and (48), we obtain

$$\sum_{m=1}^{\infty}\frac{2m-1}{\sinh^2[(2m-1)s]} = \frac{\gamma+1-\ln s}{2s^2}+O(1). \tag{49}$$

Recalling that $s=\frac{2\pi^2}{L\sqrt{Q-1}}$, for $L\gg 1$ and $\delta\ll 1$ we then obtain

$$\begin{aligned} f_2(L) = -\frac{4\delta}{\pi L}\Bigg[&\ln\left(\frac{L\sqrt{Q-1}}{2\pi^2}\right) \\ &+\gamma+1+O(1/L^2)+O(\delta)\Bigg]. \end{aligned} \tag{50}$$

for some $c>0$. Thus, within the $O(\delta^2/L)+O(\delta/L^3)+O(e^{-cL})$ errors the total energy density is

$$\begin{aligned} f(L) &\simeq \frac{2}{L}\left(4\sqrt{Q-1}-\pi\kappa\right) \\ &- \frac{4\delta}{\pi L}\left[\ln\left(\frac{L\sqrt{Q-1}}{2\pi^2}\right)+\gamma+1\right]. \end{aligned} \tag{51}$$

We now minimize the obtained expression in L. A simple calculation shows that the expression for $f(L)$ in Eq. (51) is uniquely minimized by $L = L_{\rm opt}$, where

$$L_{\rm opt} \simeq \frac{2\pi^2 e^{-\gamma}}{\sqrt{Q-1}} \exp\left[\frac{\pi}{2\delta}\left(4\sqrt{Q-1} - \pi\kappa\right)\right]. \qquad (52)$$

As expected, the optimal period is of the form appearing in Eq. (29), which justifies neglecting the error terms in the expression for $f(L)$ as $\delta \to 0$, and gives the leading order asymptotic behavior of the optimal stripe period in this limit.

B. Bloch stripes period

We can follow the same arguments as in Sec. IV A applied to the Bloch stripes for $\kappa = 0$ discussed in Sec. III B. Retracing all the computations and noticing that in this case the Fourier coefficients $a_{2m-1} = 0$ for all $m \in \mathbb{N}$, we arrive at the formula

$$f_2(L) \simeq -\frac{8\pi^3\delta}{L^3(Q-1)} \times \sum_{m=1}^{\infty}(2m-1)\mathrm{csch}^2\left(\frac{\pi^2(2m-1)}{L\sqrt{Q-1}}\right). \qquad (53)$$

An expansion analogous to the one in Sec. IV A then yields

$$f(L) \simeq \frac{2}{L}\left(4\sqrt{Q-1}\right) - \frac{4\delta}{\pi L}\left[\ln\left(\frac{L\sqrt{Q-1}}{\pi^2}\right) + \gamma + 1\right]. \qquad (54)$$

Optimizing this expression then gives, to the leading order, the optimal period

$$L_{\rm opt} \simeq \frac{\pi^2 e^{-\gamma}}{\sqrt{Q-1}} \exp\left(\frac{2\pi}{\delta}\sqrt{Q-1}\right). \qquad (55)$$

V. MICROMAGNETIC SIMULATIONS

We carried out detailed micromagnetic simulations of the magnetic stripe domains, using the open source MuMax3 software[48]. Our system consists of a box of $N_x \times 256 \times 1$ cells, where N_x is varied. The individual cell size is $l_x \times 4$ nm $\times\, l_z$, where l_x is set to 1 nm in the Bloch case (regime 1) and 0.25 nm in the Néel case (regimes 2 and 3), and $l_z = d$, where d is varied between $d = 0.65$ nm ($\delta \simeq 0.16$) and $d = 8$ nm ($\delta \simeq 2$). The choice of the number of cells in the y-direction is dictated by the MuMax3 implementation of the periodic boundary conditions for the stray field, which are approximated by specifying the number of repeats of the computational domain to define the magnetostatic kernel. We set the number of repeats in (X, Y, Z) to (5,5,0) alongside with our choice of the discretization cell sizes and numbers in order to achieve a sufficiently good accuracy of the calculation.

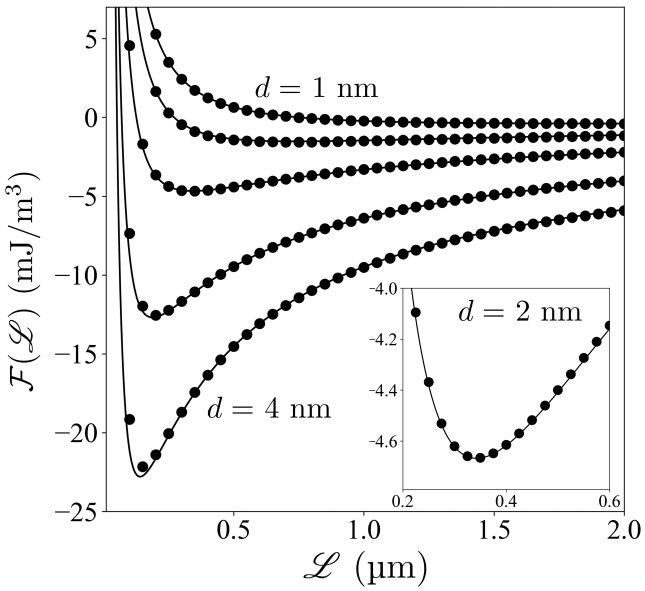

FIG. 5: Comparison between the numerical simulations in dots (MuMax3[48]) and dimensional version of the asymptotic energy $\mathcal{F}(\mathscr{L}) = f(\mathscr{L}/\ell_{\rm ex})K_d$, where $f(L)$ can be found in Eq. (51), represented as a solid line. The parameters are $A_{\rm ex} = 10$ pA/m, $M_s = 1$ MA/m, $K_{u2} = 1$ MJ/m^3 and $D_2 = 2$ mJ/m^2. The film thicknesses are (starting from the bottom curve) $d = 4$ nm, $d = 3$ nm, $d = 2$ nm, $d = 1.4$ nm and $d = 1$ nm.

We fix the system exchange constant to $A_{\rm ex} = 10$ pA/m and saturation magnetization to $M_s = 1$ MA/m, resulting in an exchange length $\ell_{\rm ex} \simeq 4$ nm. A snapshot of the simulated system in the case of Néel walls (regime 2), which has been minimized in energy, is shown in Fig. 1(a). In this simulation, the stripe period is imposed. As a consequence, in order to find the lowest energy configuration, we repeat the simulation for various N_x and look for a minimum of the energy per unit volume as a function of N_x. The equilibrium stripe period predicted by Eqs. (2) and (4) serves as a guide to guess the period in the simulation, and the simulations converge quickly to the minimum of energy for each N_x.

We extract the stripe system energy density from the simulation by suitably offsetting the total energy density output parameter of MuMax3 and compare it to the dimensional asymptotic energy density $\mathcal{F}(\mathscr{L}) = f(\mathscr{L}/\ell_{\rm ex})K_d$ in mJ/m^3, where $f(L)$ is the energy density of the stripe system computed in Sec. IV, see Eq. (51) for the Néel case and Eq. (54) for the Bloch case. In Fig. 5, we show, for regime 2 (Néel rotation, $K_{u2} = 1$ MJ/m^3 and $D_2 = 2$ mJ/m^2), the energy density (dots) obtained numerically using the `minimize` routine for the values of $N_x l_x$ between 100 nm and 2 µm and the thickness d varying from 1 nm to 4 nm. The dimensional asymptotic energy density $\mathcal{F}(\mathscr{L}) = f(\mathscr{L}/\ell_{\rm ex})K_d$ obtained from Eq. (51) and represented by the solid line in Fig. 5 shows ex-

cellent agreement with the numerical simulations. The good agreement between the asymptotics and the simulations starts to deviate around $d \simeq 4$ nm ($d \simeq L_B$).

We want to mention that in a ferromagnetic thin film, the domain wall width has been shown to be thickness-dependent, even in the ultrathin film limit[36] ($d \to 0$). In regime 1, the domain wall width estimated from a fit to the profile obtained with the micromagnetic simulations presents, for $d = 8$ nm, a 40% decrease compared to L_B. However, the excellent agreement between the micromagnetic simulations and the asymptotic formulas in this work shows that the equilibrium stripe period is unaffected by this dependence to the leading order.

VI. CONCLUSIONS

We have derived analytical formulas for the equilibrium stripe period which present an inverse exponential dependence on the film thickness and a prefactor proportional to the Bloch wall width. These formulas are derived for the case of pure Néel and Bloch rotations and are asymptotically exact for vanishing film thicknesses in the presence or absence of interfacial DMI, respectively. The formulas are applied to classical sets of system parameters, including the Bloch and the Néel regimes and a film thickness varying from one monolayer to about 10 nm. The comparison with micromagnetic simulations in the considered regimes shows excellent agreement, confirming the applicability of our formula in the ultrathin film regime. This agreement represents a quantitative improvement as compared to the state of the art formulas in the literature as previous studies did not succeed to obtain the correct asymptotics for vanishing thicknesses. The accuracy of our formulas is remarkably robust up to thicknesses of at least twice the exchange length. The variation of the wall width with the film thickness does not affect this accuracy and the formulas remain accurate as long as the thickness is smaller than the Bloch wall width. We also highlight the inapplicability, in the ultrathin film regime, of an alternative formula obtained by neglecting the wall width (thin wall approximation) which leads to a prefactor proportional to the film thickness. This settles a controversy with regards to which formula should be used for predicting the equilibrium stripe period in ultrathin films. We explicitly clarify the conditions of validity of the respective formulas as well as the proper choice of domain wall surface tension in the different regimes.

Acknowledgments

A. Bernand-Mantel was supported by France 2030 government investment plan managed by the French National Research Agency under grant reference PEPR SPIN [SPINTHEORY] ANR-22-EXSP-0009 and grant NanoX ANR-17-EURE-0009 in the framework of the Programme des Investissements d'Avenir. C. B. Muratov was supported by MUR via PRIN 2022 PNRR project P2022WJW9H and acknowledges the MUR Excellence Department Project awarded to the Department of Mathematics, University of Pisa, CUP I57G22000700001. C. B. Muratov is a member of INdAM-GNAMPA. A. Bernand-Mantel thanks N. Reyren and W. Legrand for fruitful discussions.

* Electronic address: anne.bernand-mantel@cemes.fr

[1] A. Hubert and R. Schäfer, *Magnetic Domains* (Springer, Berlin, 1998).
[2] L. D. Landau and E. M. Lifshitz, *Course of Theoretical Physics*, vol. 8 (Pergamon Press, London, 1984).
[3] C. B. Muratov, Phys. Rev. E **66**, 066108 pp. 1 (2002).
[4] A. H. Bobeck, J. Vac. Sci. Technol. **9**, 1145 (1972).
[5] J. C. Malozemov, A. and Slonczewski, *Magnetic Domain Walls in Bubble Materials* (Academic press, New-York, 1979).
[6] F. J. Himpsel, J. E. Ortega, G. J. Mankey, and R. F. Willis, Adv. Phys. **47**, 511 (1998).
[7] A. Aharoni, *Introduction to the Theory of Ferromagnetism*, vol. 109 of *International Series of Monographs on Physics* (Oxford University Press, New York, 2001), 2nd ed.
[8] U. Gradmann and J. Müller, Phys. Status Solidi B **27**, 313 (1968).
[9] H. J. G. Draaisma and W. J. M. de Jonge, J. Appl. Phys. **62**, 3318 (1987).
[10] J. R. Barnes, S. J. O'Shea, M. E. Welland, J.-Y. Kim, J. E. Evetts, and R. E. Somekh, **76**, 2974 (1994).
[11] M. T. Johnson, P. J. H. Bloemen, F. J. A. D. Broeder, and J. J. D. Vries, Rep. Prog. Phys. **59**, 1409 (1996).
[12] R. Allenspach and A. Bischof, Phys. Rev. Lett. **69**, 3385 (1992).
[13] A. Vaterlaus, C. Stamm, U. Maier, M. G. Pini, P. Politi, and D. Pescia, Phys. Rev. Lett. **84**, 2247 (2000).
[14] Y. Z. Wu, C. Won, A. Scholl, A. Doran, H. W. Zhao, X. F. Jin, and Z. Q. Qiu, Phys. Rev. Lett. **93**, 117205 (2004).
[15] A. Crépieux and C. Lacroix, J. Magn. Magn. Mater. **182**, 341 (1998).
[16] M. Bode, M. Heide, K. von Bergmann, P. Ferriani, S. Heinze, G. Bihlmayer, A. Kubetzka, O. Pietzsch, S. Blugel, and R. Wiesendanger, Nature **447**, 190 (2007).
[17] G. Chen, T. Ma, A. T. N'Diaye, H. Kwon, C. Won, Y. Wu, and A. K. Schmid, Nature Commun. **4**, 2671 (2013).
[18] W. Jiang, P. Upadhyaya, W. Zhang, G. Yu, M. B. Jungfleisch, F. Y. Fradin, J. E. Pearson, Y. Tserkovnyak, K. L. Wang, O. Heinonen, et al., Science **349**, 283 (2015).
[19] M. Schott, A. Bernand-Mantel, L. Ranno, S. Pizzini, J. Vogel, H. Béa, C. Baraduc, S. Auffret, G. Gaudin, and D. Givord, Nano Lett. **17**, 3006 (2017).
[20] R. Tomasello, E. Martinez, R. Zivieri, L. Torres, M. Carpentieri, and G. Finocchio, Sci. Rep. **4**, 6784 (2014).
[21] D. Prychynenko, M. Sitte, K. Litzius, B. Krüger, G. Bourianoff, M. Kläui, J. Sinova, and K. Everschor-Sitte, Phys.

Rev. Applied **9**, 014034 (2018).
[22] A. DeSimone, H. Knüpfer, and F. Otto, Calc. Var. PDE **27**, 233 (2006).
[23] H. Knüpfer, C. B. Muratov, and F. Nolte, Arch. Rat. Mech. Anal. **232**, 727 (2019).
[24] A. Bernand-Mantel, C. B. Muratov, and T. M. Simon, Phys. Rev. B **101**, 045416 (2020).
[25] A. Bernand-Mantel, A. Fondet, S. Barnova, T. M. Simon, and C. B. Muratov, Phys. Rev. B **108**, L161405 (2023).
[26] C. Kittel, Phys. Rev. **70**, 965 (1946).
[27] Z. Málek and V. Kamberský, Czech. J. Phys. **8**, 416 (1958).
[28] C. Kooy and U. Enz, Philips Res. Repts. **15**, 7 (1960).
[29] Y. Yafet and E. M. Gyorgy, Phys. Rev. B **38**, 9145 (1988).
[30] R. Czech and J. Villain, J. Phys. – Condensed Matter **1**, 619 (1989).
[31] D. Andelman, F. Brochard, P.-G. de Gennes, and J.-F. Joanny, C. R. Acad. Sci. Paris Sér. II **301**, 675 (1985).
[32] B. Kaplan and G. A. Gehring, J. Magn. Magn. Mater. **128**, 111 (1993).
[33] Y. Millev, J. Phys. – Condensed Matter **8**, 3671 (1996).
[34] A. B. Kashuba and V. L. Pokrovsky, Phys. Rev. B **48**, 10335 (1993).
[35] A. Sukstanskii and K. Primak, J. Magn. Magn. Mater. **169**, 31 (1997).
[36] I. Lemesh, F. Büttner, and G. S. D. Beach, Phys. Rev. B **95**, 174423 (2017).
[37] T. N. G. Meier, M. Kronseder, and C. H. Back, Phys. Rev. B **96**, 144408 (2017).
[38] R. Hoffmann, D. Bürgler, P. Van Schendel, H. Hug, S. Martin, and H.-J. Güntherodt, J. Magn. Magn. Mater. **250**, 32 (2002).
[39] N. Bergeard, J.-P. Jamet, J. Ferré, A. Mougin, and J. Fassbender, J. Appl. Phys. **108**, 103915 (2010).
[40] S.-G. Je, P. Vallobra, T. Srivastava, J.-C. Rojas-Sánchez, T. H. Pham, M. Hehn, G. Malinowski, C. Baraduc, S. Auffret, G. Gaudin, et al., Nano Lett. **18**, 7362 (2018).
[41] C. Bouard, P. Warin, A. Marty, L. Vila, V. T. Pham, and J.-P. Attané, AIP Adv. **8**, 095315 (2018).
[42] M. Schott, L. Ranno, H. Béa, C. Baraduc, S. Auffret, and A. Bernand-Mantel, J. Magn. Magn. Mater. **520**, 167122 (2021).
[43] C. Balan, J. W. Van Der Jagt, A. Fassatoui, J. Peña Garcia, V. Jeudy, A. Thiaville, M. Bonfim, J. Vogel, L. Ranno, D. Ravelosona, et al., Small **19**, 2302039 (2023).
[44] F. Ando, H. Kakizakai, T. Koyama, K. Yamada, M. Kawaguchi, S. Kim, K.-J. Kim, T. Moriyama, D. Chiba, and T. Ono, Appl. Phys. Lett. **109**, 022401 (2016).
[45] T. Dohi, S. Kanai, A. Okada, F. Matsukura, and H. Ohno, AIP Adv. **6**, 075017 (2016).
[46] S. Yang, K.-W. Moon, T.-S. Ju, C. Kim, S. Park, and C. Hwang, J. Magn. Magn. Mater. **539**, 168381 (2021).
[47] R. Skomski, H.-P. Oepen, and J. Kirschner, Phys. Rev. B **58**, 3223 (1998).
[48] A. Vansteenkiste, J. Leliaert, M. Dvornik, M. Helsen, F. Garcia-Sanchez, and B. Van Waeyenberge, AIP Adv. **4**, 107133 (2014).
[49] A. Thiaville, S. Rohart, E. Jué, V. Cros, and A. Fert, Europhys. Lett. **100**, 57002 (2012).
[50] C. B. Muratov and V. V. Slastikov, Proc. R. Soc. A **473**, 20160666 (2017).
[51] S. Tarasenko, A. Stankiewicz, V. Tarasenko, and J. Ferré, J. Magn. Magn. Mater. **189**, 19 (1998).
[52] B. Heinrich and J. F. Cochran, Adv. Phys. **42**, 523 (1993).
[53] J.-F. Babadjian, G. Di Fratta, I. Fonseca, G. A. Francfort, M. Lewicka, and C. B. Muratov, Quart. Appl. Math **81** (2023).
[54] G. Di Fratta, C. B. Muratov, and V. V. Slastikov, Math. Models Methods Appl. Sci. **34**, 1861 (2024).
[55] G. Di Fratta, C. B. Muratov, F. N. Rybakov, and V. V. Slastikov, SIAM J. Math. Anal. **52**, 3580 (2020).
[56] C. B. Muratov and V. V. Osipov, J. Comp. Phys. **216**, 637 (2006).
[57] C. B. Muratov and V. V. Osipov, J. Appl. Phys. **104**, 053908 (2008).
[58] A. Giuliani, J. L. Lebowitz, and E. H. Lieb, Commun. Math. Phys. **286**, 163 (2009).
[59] C. B. Muratov and X. Yan, Proc. R. Soc. A **472**, 20150762 (2016).
[60] S. Banerjee and B. Wilkerson, Int. J. Number Theory **13**, 2097 (2017).
[61] J. C. Kluyver, KNAW Proceedings **22**, 323 (1919).